Supporting Information

Extraordinary role of Hg in enhancing thermoelectric performance of p-type SnTe

Gangjian Tan,[1] Fengyuan Shi,[2] Jeff W. Doak,[2] Hui Sun,[3] Li-Dong Zhao,[1] Pengli Wang,[1] Ctirad Uher,[3] Chris Wolverton,[2] Vinayak P. Dravid,[2] and Mercouri G. Kanatzidis[1.4,*]

[1]*Department of Chemistry, Northwestern University, Evanston, Illinois 60208, United States*

[2]*Department of Materials Science and Engineering, Northwestern University, Evanston, Illinois 60208, United States*

[3]*Department of Physics, University of Michigan, Ann Arbor, Michigan 48109, United States*

[4]*Materials Science Division, Argonne National Laboratory, Argonne, Illinois 60439, United States*

*Corresponding author: m-kanatzidis@northwestern.edu

Table S1. Room temperature density ρ for $Sn_{0.98}Bi_{0.02}Te$-x%HgTe and $Sn_{0.98}Bi_{0.02}Te$-2% CdTe samples.

Sample composition	Density ρ (g/cm^3)
$Sn_{0.98}Bi_{0.02}Te$	6.2715
$Sn_{0.98}Bi_{0.02}Te$-0.5%HgTe	6.2687
$Sn_{0.98}Bi_{0.02}Te$-1%HgTe	6.3124
$Sn_{0.98}Bi_{0.02}Te$-2%HgTe	6.2565
$Sn_{0.98}Bi_{0.02}Te$-3%HgTe	6.2058
$Sn_{0.98}Bi_{0.02}Te$-4%HgTe	6.2216
$Sn_{0.98}Bi_{0.02}Te$-2%CdTe	6.2949

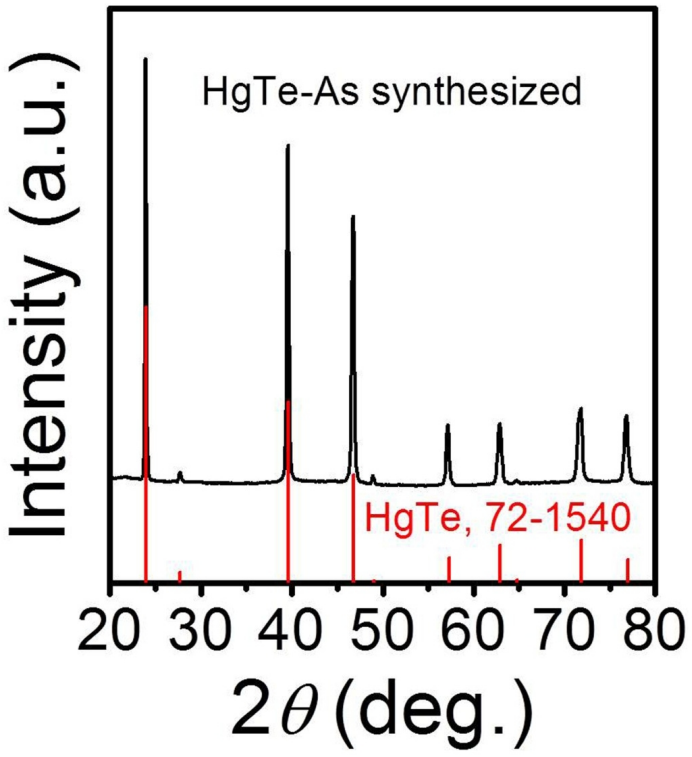

Figure S1. Powder XRD pattern of as-synthesized HgTe. The Bragg peaks correspond well with the standard diffraction patterns of HgTe (JCPDS Card #72-1540).

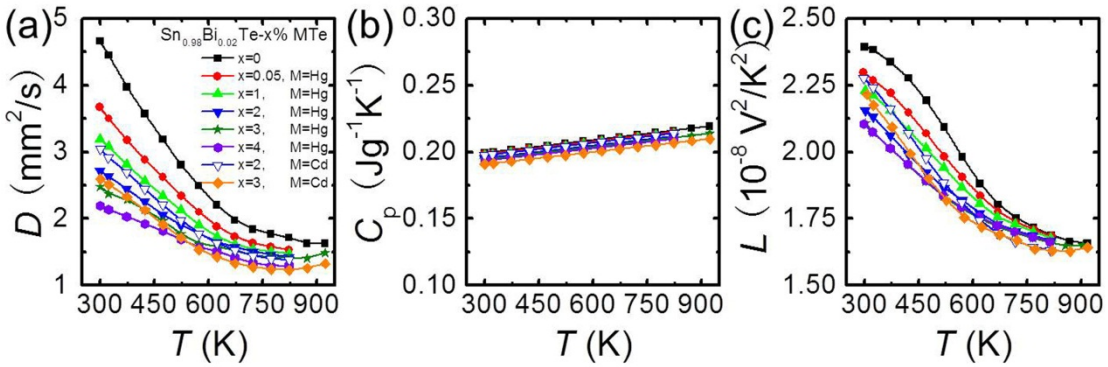

Figure S2. (a) Thermal diffusivity D, (b) heat capacity C_p, and (c) Lorenz number L as a function of temperature for $Sn_{0.98}Bi_{0.02}Te$-x%HgTe/CdTe samples.

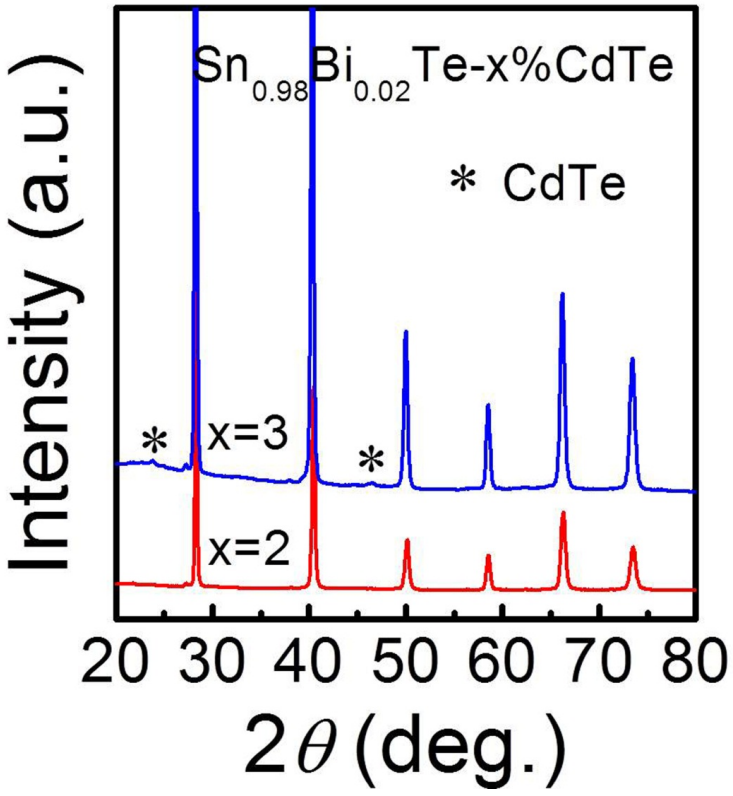

Figure S3. Powder XRD pattern of $Sn_{0.98}Bi_{0.02}Te$-x%CdTe.

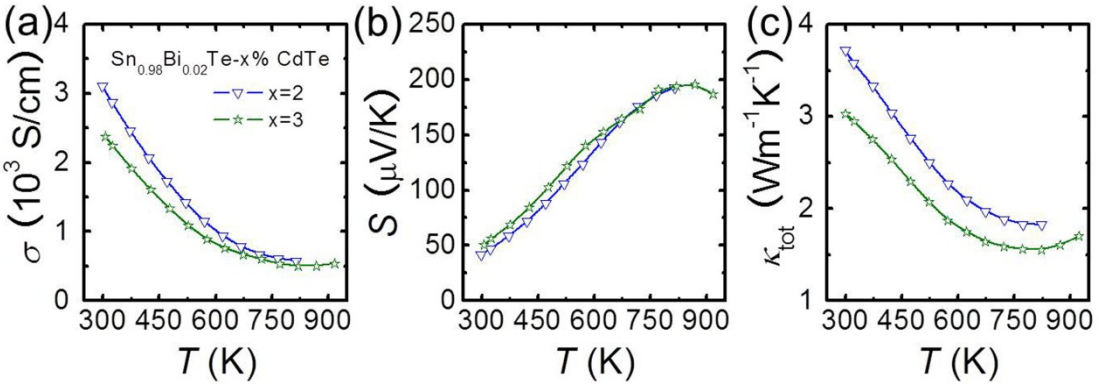

Figure S4. Temperature dependent (a) electrical conductivity, (b) Seebeck coefficient, and (c) thermal conductivity for $Sn_{0.98}Bi_{0.02}Te$-x%CdTe.

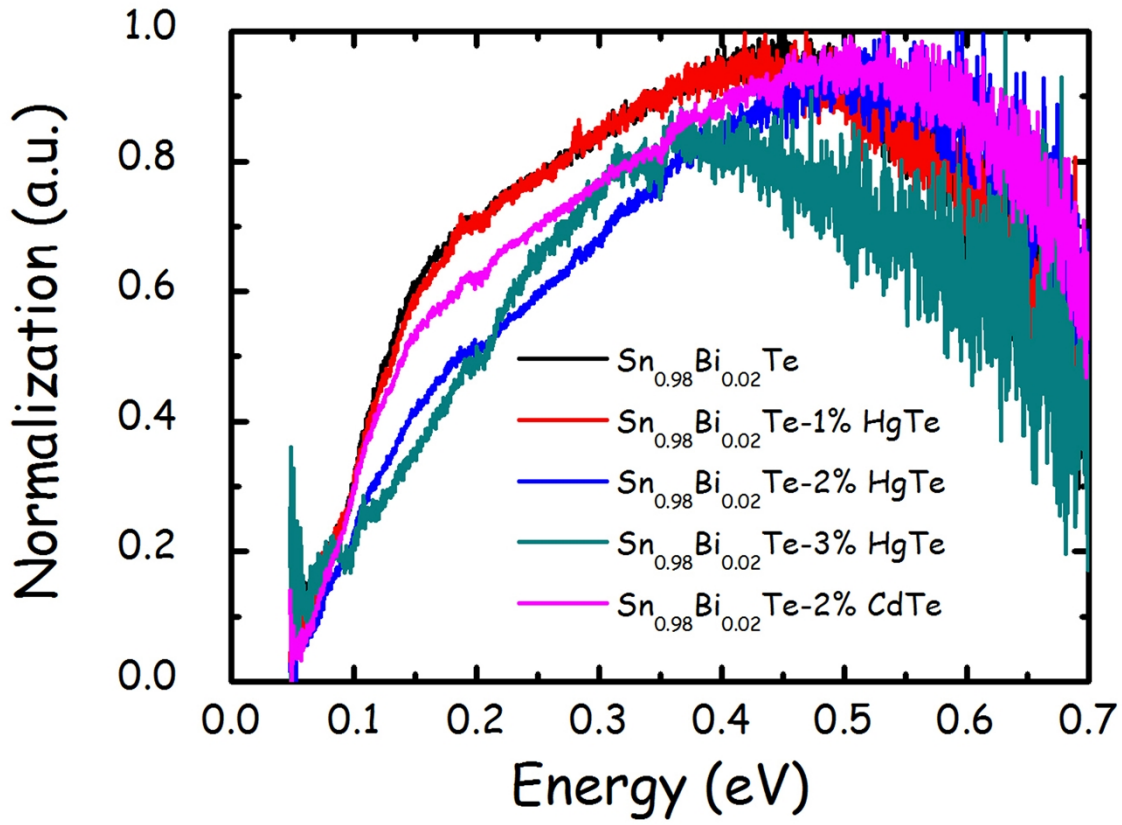

Figure S5. Electronic absorption spectra for $Sn_{0.98}Bi_{0.02}Te$-x%(Hg,Cd)Te.

Evident band gaps cannot be derived from the spectra because of the strong interference from a large amount of free carriers (Zemel, J.; Jensen, J.; Schoolar, R. Phys. Rev. 1965, 140, A330; Tan, G. et al, J. Am. Chem. Soc. 2014, 136, 7006-7017; Banik, A. et al., J. Mater. Chem. A 2014, 2, 9620-9625). However, the gradual shift of the absorption edges towards higher energy with increasing HgTe/CdTe content indicates the increase of band gaps.

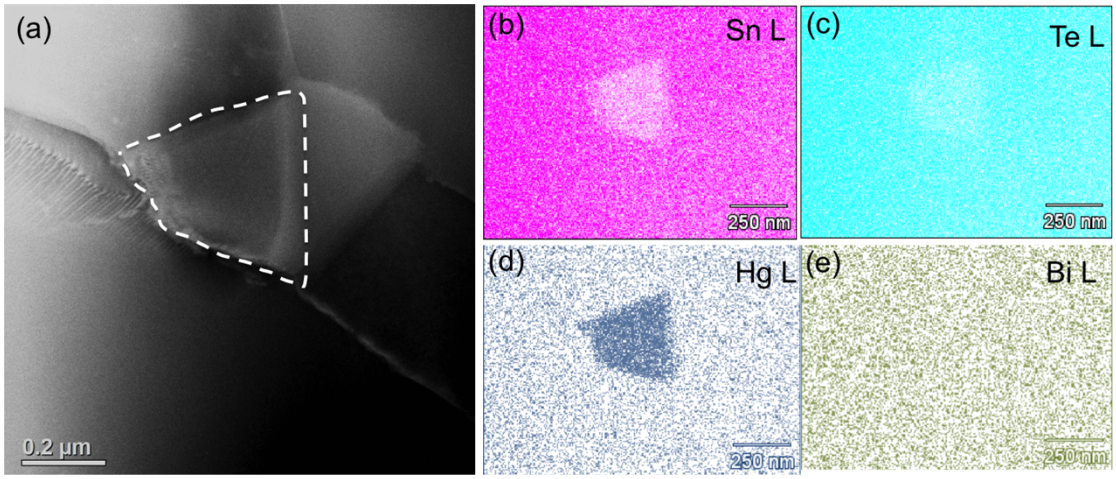

Figure S6. STEM EDS spectrum image (SI) of $Sn_{0.98}Bi_{0.02}Te$-3%HgTe. (a) A low magnification STEM image shows an Hg rich particle at a grain boundary junction, highlighted by the dashed white line. (b)-(e) are EDS mappings for elements Sn, Te, Hg and Bi, respectively. Darker in color in the elementary maps corresponds to higher concentrations.

STEM EDS spectrum image (SI) was taken to investigate the elements distributions of specimen $Sn_{0.98}Bi_{0.02}Te$-3%HgTe. A low magnification STEM image in Figure S6 (a) has shown an HgTe particle with size ~400 nm at a triple grain boundary junction. STEM EDS SI in Figure S6 (b)-(e) shows that the HgTe particle is rich in Hg but deficient in Sn; Te and Bi are also almost uniform in both the HgTe precipitate and the matrix. The HgTe particles prefer to occupy along grain boundaries, which may be due to the high mobility nature of Hg. The EDS quantification based on the integrated EDS SI shows the atomic composition: Sn:Te ~1 and Bi is 1.3% and Hg is ~3%. The EDS quantification results show no significant loss of Hg or Bi elements.

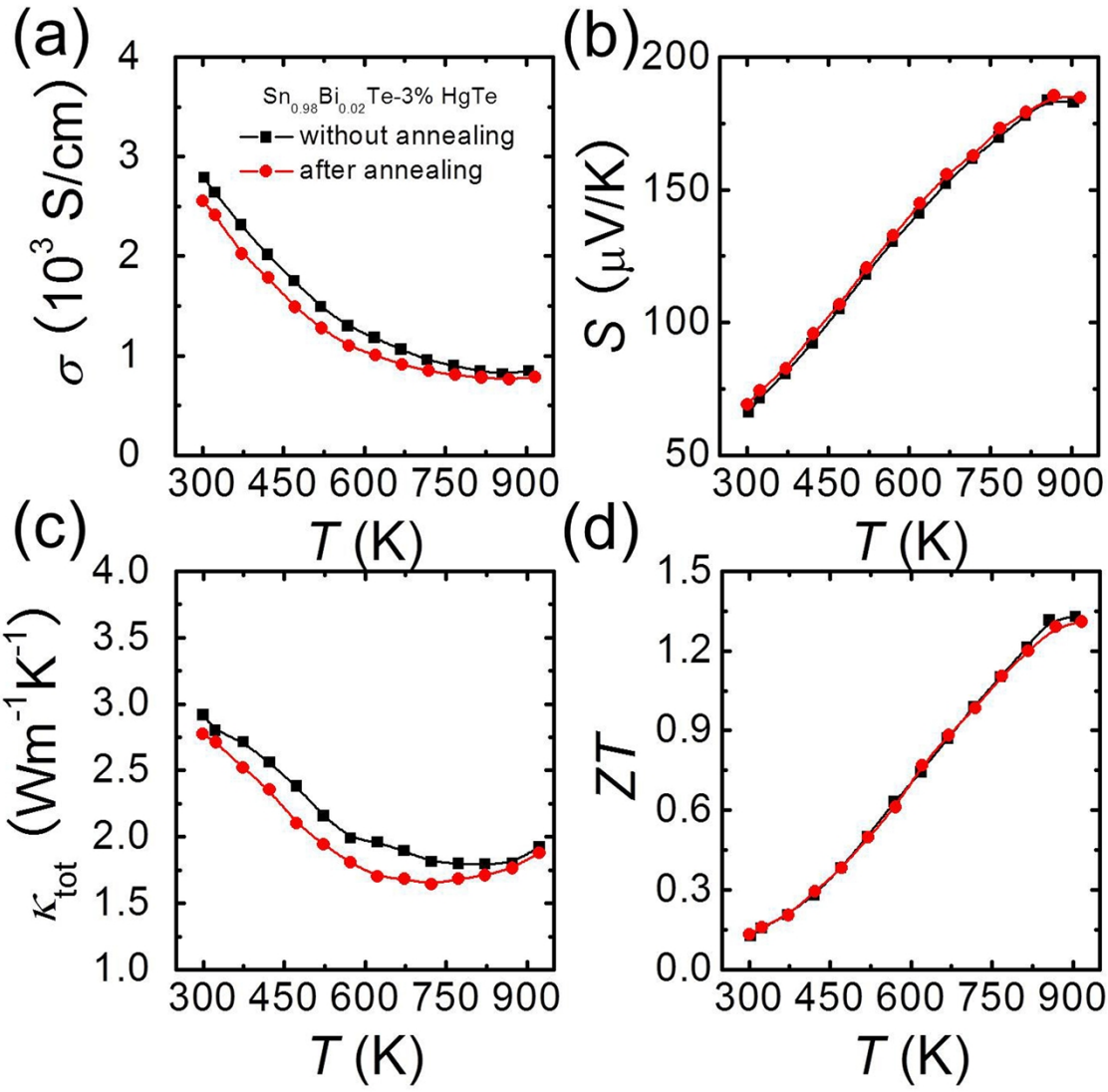

Figure S7. Temperature dependent thermoelectric transport properties for sample $Sn_{0.98}Bi_{0.02}Te$-3%HgTe before (black square) and after (red circle) vacuum annealing at 723 K for 7 days: (a) electrical conductivity; (b) Seebeck coefficient; (c) total thermal conductivity, and (d) *ZT* values. Clearly, the high performance material is quite stable.